

# Sub-kilohertz intrinsic linewidth stimulated Brillouin laser in integrated lithium niobate microresonators

Chuntao Li<sup>1,4,#</sup>, Jiale Deng<sup>2,#</sup>, Xingzhao Huang<sup>2,#</sup>, Xiaochao Luo<sup>3,5</sup>, Renhong Gao<sup>4</sup>, Jintian Lin<sup>3,5,\*</sup>, Huakang Yu<sup>2,†</sup>, Jianglin Guan<sup>1,4</sup>, Zhiyuan Li<sup>2</sup>, and Ya Cheng<sup>1,3,4,6,7,8,9,‡</sup>

<sup>1</sup>*State Key Laboratory of Precision Spectroscopy, East China Normal University, Shanghai 200062, China.*

<sup>2</sup>*School of Physics and Optoelectronics, State Key Laboratory of Luminescent Materials and Devices, South China University of Technology, Guangzhou 510460, People's Republic of China*

<sup>3</sup>*State Key Laboratory of High Field Laser Physics, Shanghai Institute of Optics and Fine Mechanics, Chinese Academy of Sciences, Shanghai 201800, China.*

<sup>4</sup>*The Extreme Optoelectromechanics Laboratory (XXL), School of Physics and Electronic Science, East China Normal University, Shanghai 200241, China*

<sup>5</sup>*University of Chinese Academy of Sciences, Beijing 100049, China.*

<sup>6</sup>*Shanghai Research Center for Quantum Sciences, Shanghai 201315, China*

<sup>7</sup>*Hefei National Laboratory, Hefei 230088, China*

<sup>8</sup>*Collaborative Innovation Center of Extreme Optics, Shanxi University, Taiyuan 030006, China*

<sup>9</sup>*Collaborative Innovation Center of Light Manipulations and Applications, Shandong Normal University, Jinan 250358, China*

<sup>#</sup>*Chuntao Li, Jiale Deng, and Xingzhao Huang contributed equally to this work.*

\**jintianlin@siom.ac.cn*

†*hkyu@scut.edu.cn*

‡*ya.cheng@siom.ac.cn*

**arXiv @ Nov. 2024**

## Abstract

The rapid advancement of lithium niobate on insulator (LNOI) photonics has spurred interest in approaches to develop ultra-narrow linewidth Brillouin microlasers. Here we demonstrate an integrated Brillouin microlaser with 118-Hz intrinsic linewidth and 3.15-mW threshold power in a dispersion engineered and suspended LNOI microdisk resonator of 116  $\mu\text{m}$  diameter. Benefited from the ultrahigh Q factor and sub-millimeter-scale microresonator, large Brillouin gain is attained via the backward intermodal stimulated Brillouin scattering between the dual-resonant optical WGMs and a 10-GHz whispering-gallery mechanical mode, while satisfying the requirements of both energy and momentum conservations. Such strong optomechanical coupling rate up to 12.1 kHz approaching the highest reported efficiency is readily for a record narrow linewidth and a lowest stimulated Brillouin laser threshold value within sub-millimeter-scale integrated microresonators reported so far. This advancement in integrated ultra-narrow linewidth Brillouin lasers with compact cavity size paves the way for applications ranging from coherent information processing to precision metrology within the realm of high density photonic integration.

Lithium niobate on insulator (LNOI) wafer has been considered as one of the most important photonic platforms for a wide range of cutting-edge applications ranging from high capability data processing to miniaturized precision metrology, benefited from the outstanding optoelectronic properties featuring large second-order nonlinearity and high Pockels electro-optic coefficient [1-9]. The rapid advancement of LNOI photonics has spurred interest in approaches to develop ultra-narrow linewidth Brillouin microlasers with low-threshold power, which have been demonstrated in other photonic platforms like silicon nitride [10-16]. The conventional strategy for realization of integrated Brillouin lasers is to use a whispering gallery mode (WGM) microlaser cavity that has ultrahigh Q factor ( $> 10^6$ ), and whilst large cavity (millimeter-to-centimeter scale) with its free spectral range matching the Brillouin gain shift. However, the fabrication of such large LNOI cavity with ultrahigh Q factor still poses significant challenges, not to mention its large mode volume, relatively low Q factors and substrate-induced dissipation which are unfavored for low-threshold operation, efficient optomechanical coupling, and high-density photonic integration [13].

The stimulated Stokes Brillouin lasing was demonstrated in a dispersion-engineered and suspended LNOI microdisk resonator by injecting continuous-wave (CW) pump light. The experimental setup was schematically illustrated in Fig. 1 (see [Supplementary S1](#) for detailed information). We designed and fabricated the dispersion-engineered suspended microdisks with the aim to realize the dual-resonance condition for matching the narrow Brillouin gain shift. Since the Brillouin gain shift of  $\sim 10$  GHz is quite small, the principle of inter-modal stimulated Brillouin scattering

(SBS) has to be applied, where two sets of cavity modes with different radial quantum numbers were involved [17]. The suspended LNOI microdisks were fabricated with a radius of 58.5  $\mu\text{m}$ , a thickness of 800 nm, and a wedge angle of the sidewall of  $15^\circ$  by femtosecond laser photolithography assisted chemo-mechanical etching [18], sitting on smaller silicon dioxide pillars, as depicted in the inset of Fig. 1. It is of particular concern that the periphery of the resonator is suspended in air [19-21], which readily provides tight confinements of both optical and acoustic modes [19,22] inside the microresonator. For the 116- $\mu\text{m}$ -diameter of LNOI microresonator and TE-polarized optical WGMs used in the experiment, the corresponding free spectral ranges (FSR) are around 445 GHz for the  $\text{TE}_0$  mode and 420 GHz for the  $\text{TE}_3$  mode. As the FSRs of the  $\text{TE}_3$  and  $\text{TE}_0$  modes differ by 4.5 %, dual-resonance condition of the pump of the  $\text{TE}_3$  mode and Stokes light of the  $\text{TE}_0$  mode become accessible every 60 nm over the wavelength tuning range (from 1510 nm to 1610 nm). Moreover, in addition to facilitate the Brillouin laser around 1555 nm, fine dispersion trimming was achieved by elaborately coupling the microdisk with a tapered optical fiber to tune the resonant frequency interval of the two optical WGMs (see [Supplementary S2](#)). Interacting with the fruitful acoustic modes in the frequency range around 10 GHz (see [Supplementary S3](#)), it is readily expected that the resonance frequency condition could be satisfied for the SBS while precisely tuning the wavelength of incident pump light.

To realize Stokes Brillouin laser (SBL), the CW pump light at the wavelength of 1555.81 nm was injected into the LNOI microresonator. To access the  $\text{TE}_3$  cavity modes, the tapered fiber was subtly placed in contact with the edge of the microdisk for high-

order optical WGM excitation by carefully adjusting the coupling position. While increasing the input power of pump light, a backward SBL signal could be observed at the wavelength of 1555.89 nm recorded by an optical spectral analyzer (OSA), as shown in Figs. 2(a). From the spectrum, we found that the wavelength interval between the pump wavelength and the SBL signal was  $\sim 0.08$  nm, corresponding to Brillouin shift  $\Omega_B$  of  $\sim 10$  GHz. This Brillouin shift  $\Omega_B$ , equal to the radio-frequency (RF) beat note signal of the pump light and the backward SBL, was further identified at a frequency centered at 10.3 GHz using a high-speed photodetector (PD) connected with a real-time electrical spectral analyzer (ESA), as shown in Fig. 2(b). The dependence of the backward SBL power on the on-chip pump power was also measured, as shown in Fig. 2(c). Above the pump threshold of 3.15 mW, the SBL power grows linearly with the increasing pump power, which agrees well with the nature of SBS process. From linear fitting, the slope efficiency was determined as high as 6.8%. According to the theory of SBL threshold as in the supporting information, for the over-coupled condition in the experiment, we may obtain Brillouin gain  $G_B = 0.093 (m \cdot W)^{-1}$  for pump light of  $\lambda = 1555.8 \text{ nm}$  and cavity length of  $L = \pi \cdot 116 \mu\text{m}$ . As the coupling plays an important role in determining the SBL threshold (see [Supplementary S4](#)), even lower threshold could be possible if we further optimize the tapered fiber coupling [14,17].

To understand the experimental observations, we derived both analytical and numerical models that describe the behavior of SBL oscillation inside the LNOI microresonators, as shown in Fig. 3. It is known that both shear and longitudinal

acoustic waves exist in such a microresonator with its periphery suspending in air. As the measured value of Brillouin shift around 10.3 GHz, one could readily identify that the shear acoustic wave was involved in the SBS process. This is because  $V_A$  of the shear acoustic wave in lithium niobate around 3600 m/s [19], corresponding to a calculated Brillouin shift  $\Omega_B = \frac{4\pi n V_A}{\lambda_p}$  to be  $2\pi \cdot 10.1$  GHz, a value close to the experimental results. For the LNOI microresonator with diameter of  $116 \mu\text{m}$ , the modal dispersion was plotted in Fig. 3 (b). It is found that pump light of TE<sub>3</sub>-polarized mode (1588.808 nm,  $m = 433$  is the azimuthal number) and the Stokes light of TE<sub>0</sub>-polarized mode (1555.892 nm,  $m = 458$ ) are interacting with a mechanical WGM (10.1 GHz) to mediate the intermodal Brillouin scattering. The discrepancy of Brillouin shift,  $\sim 0.2$  GHz, between simulation and experiment was possibly caused by imperfection of fabrications and the anisotropy of LNOI microresonator (such as photoelastic and stiffness tensors) that was not considered in the simulation.

To characterize the strength of stimulated Brillouin scattering, the single-photon optomechanical coupling rate  $g_0$  can be derived [23],

$$g_0 = -\frac{\omega_p x_{zpf}}{2} (\int f_{mb}^{cav} dA + \int f_{pe}^{cav} dV), \quad (1)$$

where  $x_{zpf} = \sqrt{\hbar / (2m_{eff}\Omega)}$  is the zero-point fluctuation of the mechanical mode with effective mass  $m_{eff} = \int \rho |\mathbf{u}_m|^2 / \max |\mathbf{u}_m|^2 dV$ ,  $f_{mb}^{cav}$  and  $f_{pe}^{cav}$  denote the area and volume overlap integrands representing the moving boundary (MB) and photoelastic (PE) contributions, respectively. Optomechanical coupling between the calculated optical modes and mechanical mode can be quantitatively investigated by taking a look at the individual components of the overlap integrals during the calculation of  $g_0$  [25].

For efficient optomechanical coupling between the pump light with antisymmetric modal profile (TE<sub>3</sub> mode, as shown in Fig. S2 (a), see [Supplementary S3](#)) and the Stokes light with symmetric modal profile (TE<sub>0</sub> mode, as shown in Fig. S2 (b)), a mechanical mode with anti-symmetry (as shown in Fig. S4 (d)) was required so as to mediate the intermodal Brillouin scattering with maximized  $g_0$  up to 12.1 kHz. This value approaches the-state-of-the-art result (i.e., 12.5 kHz) reported in a sophisticated micron-sized supermode microresonator [13], which is benefited from the utilization of the sub-millimeter-scale microresonator. Detailed analysis can be found in [Supplementary S3](#).

The frequency noises of the pump laser and the backward SBL measured by the commercially available laser phase noise analyzer based on correlated self-heterodyne method [13] are shown in Fig. 4(a). The white-frequency-noise floors  $N_{wfn}$  of the pump laser and the backward SBL were measured to be 546.4 Hz<sup>2</sup>/Hz and 37.4 Hz<sup>2</sup>/Hz, revealing short-term linewidths  $L_{st}$  of 1716.6 Hz and 117.5 Hz ( $L_{st} = N_{wfn} \times \pi$ ) [26], respectively. And the dependence of the short-term linewidth of the SBL on the SBL power was also characterized, as the results plotted in Fig. 4(b). The linewidth almost linearly increases as the growth of the SBL power, confirming that the linewidth corresponds to intrinsic linewidth. Such ultra-narrow linewidth is resulted from the narrow Brillouin gain bandwidth and the short lifetime of the Brillouin phonon [10,12]. For comparison with previous results obtained without accounting for the effects of optical coherence—arising from the length-limited delay in self-heterodyne narrow-linewidth signals, as described in Ref. [16], the phase noise and intrinsic linewidth of

the SBL, measured using a custom-built optical delayed self-heterodyne interferometer, are presented in [Supplementary S5](#). These measurements revealed an underestimated intrinsic linewidth of approximately 0.5 Hz.

Theoretically, the linewidth of SBL can be given by [25],

$$\Delta\nu_{SBL} = \frac{\Gamma^2}{(\gamma + \Gamma)^2} \frac{\hbar\omega_s^3}{4\pi Q_T Q_{ex} P_{SBL}} n_{th} + \frac{\gamma^2}{(\gamma + \Gamma)^2} \Delta\nu_{pump} \quad (2)$$

where the first part represents the fundamental linewidth and second part represents the contributing factor of linewidth from the transferred pump noise. If the linewidth of pump laser is relatively large or satisfying the condition of mechanical lasing [23] (i.e.,  $\gamma_s \gg \Gamma_m$ ), the linewidth of SBL was mainly contributed by the pump noise. If stokes mode dissipation is far smaller than mechanical mode dissipation ( $\gamma_s \ll \Gamma_m$ ), stokes field would experience linewidth-narrowing [26]. If we take the measured values of  $Q_T = 4.69 \times 10^6$ ,  $P_{SBL} = 1.27 \text{ mW}$ ,  $Q_{ex} = 5.53 \times 10^6$ , then we have fundamental linewidth  $\sim 277 \text{ Hz}$  (see [Supplementary S6 for details](#)). As  $\gamma_s \ll \Gamma_m$  in our experiment, the influence due to the linewidth of pump light would be insignificant, giving rise to a final linewidth mainly contributed by the fundamental linewidth, which is in good agreement with the measured SBL linewidth (118 Hz). Further improvement of Q factor of the microcavity would enable narrower SBL laser linewidth even to sub-hertz level [10,27].

Our measured spectrum shows only the Stokes Brillouin lasing process and the absence of anti-Stokes process. This is reasonable that current inter-modal Brillouin scattering configuration cannot guarantee simultaneous fulfillment of phase matching condition for the anti-Stokes Brillouin lasing process. Thus, the Stokes and anti-Stokes



processes was effectively decoupled, leading to efficient single-sideband Stokes gain with 6.8% slope efficiency [28]. Further improvement of the cavity design could facilitate the simultaneous harnessing of both Stokes and anti-Stokes Brillouin scattering processes, by incorporating more than two sets of cavity modes into the nonlinear Brillouin interactions.

In conclusion, an ultra-narrow intrinsic linewidth photonic integrated stimulated Brillouin laser is demonstrated with high-frequency Brillouin gain shift  $>10$  GHz in a small integrated LNOI microdisk resonator for the first time, demonstrating the lowest threshold values and highest conversion efficiency of 6.8% reported in sub-millimeter-scale integrated microresonators. And the intrinsic linewidth reaches only 118 Hz in good agreement with the theoretical prediction. This breakthrough in integrated ultra-narrow linewidth Brillouin lasers with compact cavity lengths paves the way for applications ranging from coherent information processing to precision metrology within the realm of high density photonic integration.

We thank Peking university Yangtze delta institute of optoelectronics for providing the laser phase noise measurement system (iFN5000).

### **References:**

- [1] Z. Xie, F. Bo, J. Lin, H. Hu, X. Cai, X. Tian, Z. Fang, J. Chen, M. Wang, F. Chen, Y. Cheng, J. Xu, and S. Zhu, *Adv. Phys. X* **9**, 2322739 (2024).
- [2] Y. Jia, L. Wang, and F. Chen, *Appl. Phys. Rev.* **8**, 011307 (2021).

- [3] D. Zhu, L. Shao, M. Yu, R. Cheng, B. Desiatov, C. J. Xin, Y. Hu, J. Holzgrafe, S. Ghosh, A. Shams-Ansari, E. Puma, N. Sinclair, C. Reimer, M. Zhang, and M. Lončar, *Adv. Opt. Photon.* **13**, 242 (2021).
- [4] G. Chen, N. Li, J. D. Ng, H.-L. Lin, Y. Zhou, Y. H. Fu, L. Y. T. Lee, Y. Yu, A.-Q. Liu, and A. J. Danner, *Adv. Photon.* **4**, 034003 (2022).
- [5] J. Lin, F. Bo, Y. Cheng, and J. Xu, *Photon. Res.* **8**, 1910 (2020).
- [6] Q. Luo, F. Bo, Y. Kong, G. Zhang, and J. Xu, *Adv Photon.* **5**, 034002 (2023).
- [7] M. Li, L. Chang, L. Wu, J. Staffa, J. Ling, U. A. Javid, S. Xue, Y. He, R. Lopez-Rios, T. J. Morin, H. Wang, B. Shen, S. Zeng, L. Zhu, K. J. Vahala, J. E. Bowers, and Q. Lin, *Nat. Commun.* **13**, 5344 (2022).
- [8] Y. Zhao, X. Liu, K. Yvind, X. Cai, and M. Pu, *Commun. Phys.* **6**, 350 (2023).
- [9] K. Ye, H. Feng, R. te Morsche, A. Mishra, Y. Klaver, C. Wei, Z. Zheng, A. Keloth, A. T. Işık, Z. Chen, C. Wang, D. Marpaung, arXiv preprinted arXiv: 2311.14697 (2023).
- [10] S. Gundavarapu, G. M. Brodrik, M. Puckett, T. Huffman, D. Bose, R. Behunin, J. Wu, T. Qiu, C. Pinho, N. Chauhan, J. Nohava, P. T. Rakich, K. D. Nelson, M. Salit, and D. J. Blumenthal, *Nat. Photonics* **13**, 60 (2019).
- [11] K. Y. Yang, D. Y. Oh, S. H. Lee, Q.-F. Yang, X. Yi, B. Shen, H. Wang, and K. Vahala, *Nat. Photonics* **12**, 297 (2018).
- [12] B. J. Eggleton, C. G. Poulton, P. T. Rakich, M. J. Steel, and G. Bahl, *Nat. Photonics* **13**, 664 (2019).
- [13] M. Wang, Z.-G. Hu, C. Lao, Y. Wang, X. Jin, X. Zhou, Y. Lei, Z. Wang, W. Liu,

- Q.-F. Yang, and B.-B. Li, *Phys. Rev. X* **14**, 011056 (2024).
- [14] Y. Bai, M. Zhang, Q. Shi, S. Ding, Y. Qin, Z. Xie, X. Jiang, and M. Xiao, *Phys. Rev. Lett.* **126**, 063901 (2021).
- [15] S. Zhu, B. Xiao, B. Jiang, L. Shi, and X. Zhang, *Nanophotonics* **8**, 931 (2019).
- [16] Y. Li, D. Xia, H. Cheng, L. Luo, L. Wang, S. Zeng, S. Yang, L. Li, B. Chen, B. Zhang, and Z. Li, *Opt. Lett.* **49**, 4529 (2024).
- [17] N. Chauhan, A. Isichenko, K. Liu, J. Wang, Q. Zhao, R. O. Behunin, P. T. Rakich, A. M. Jayich, C. Fertig, C. W. Hoyt, and D. J. Blumenthal, *Nat. Commun.* **12**, 4685 (2021).
- [18] R. Wu, J. Zhang, N. Yao, W. Fang, L. Qiao, Z. Chai, J. Lin, and Y. Cheng, *Opt. Lett.* **43**, 4116 (2018).
- [19] C. C. Rodrigues, R. O. Zurita, T. P. M. Alegre, and G. S. Wiederhecker, *J. Opt. Soc. Am. B* **40**, D56 (2023).
- [20] Y.-H. Yang, J.-Q. Wang, Z.-X. Zhu, X.-B. Xu, Q. Zhang, J. Lu, Y. Zeng, C.-H. Dong, L. Sun, G.-C. Guo, and C.-L. Zou, *Sci. China Phys. Mech. Astron.* **67**, 214221 (2024).
- [21] W. Wang, Y. Yu, Y. Li, Z. Bai, G. Wang, K. Li, C. Song, Z. Wang, S. Li, Y. Wang, Z. Lu, Y. Li, T. Liu, and X. Yan, *Appl. Sci.* **11**, 8390 (2021).
- [22] M. S. Kang, A. Nazarkin, A. Brenn, and P. S. J. Russell, *Nat. Physics* **5**, 276 (2009).
- [23] G. S. Wiederhecker, P. Dainese, and T. P. Mayer Alegre, *APL Photonics* **4**, 071101 (2019).
- [24] D. Xu, F. Yang, D. Chen, F. Wei, H. Cai, Z. Fang, and R. Qu, *Opt. Express* **23**,

22386 (2015).

- [25] Z. Yuan, H. Wang, L. Wu, M. Gao, and K. Vahala, *Optica* **7**, 1150 (2020).
- [26] N. T. Otterstrom, R. O. Behunin, E. A. Kittlaus, Z. Wang, and P. T. Rakich, *Science* **360**, 1113 (2018).
- [27] J. Li, H. Lee, T. Chen, and K. J. Vahala, *Opt. Express* **20**, 20170 (2012).
- [28] E. A. Kittlaus, N. T. Otterstrom, and P. T. Rakich, *Nat. Commun.* **8**, 15819 (2017).

### Captions of figures:

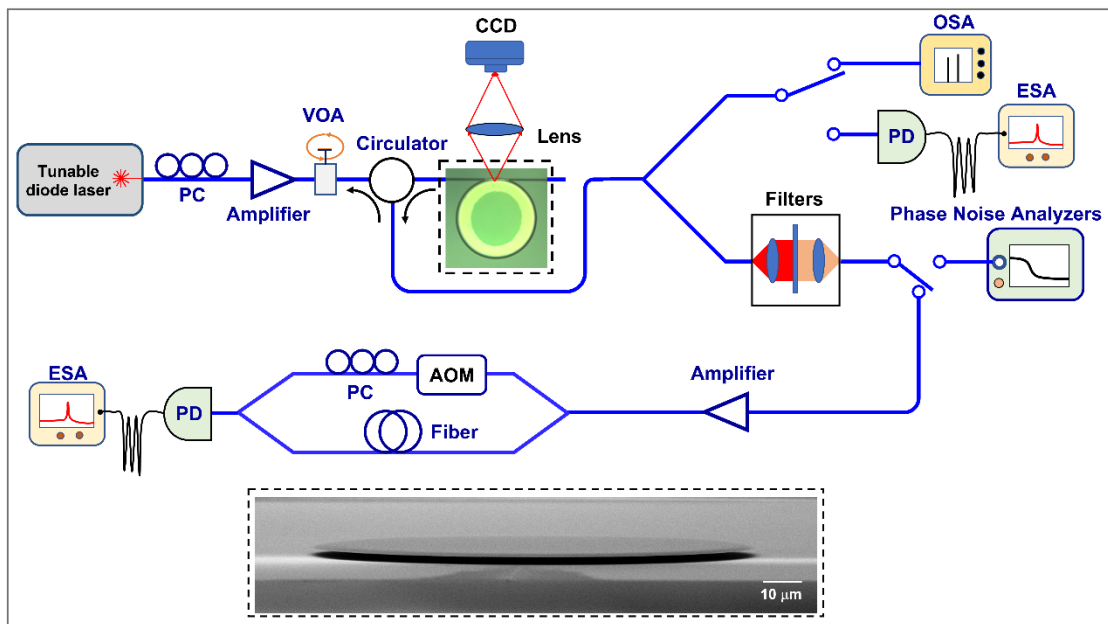
Fig. 1 (Color online) (a) Experimental setup for generating the Brillouin microlaser. Here, acoustic-optic modulator (AOM) which shifted the light frequency by 100 MHz is denoted as AOM. And polarization controller, erbium-doped fiber amplifier, and variable optical attenuator are denoted as PC, amplifier, and VOA, respectively. Inset: Scanning-electron-microscope (SEM) image of the microresonator.

Fig. 2 (Color online) (a) Optical spectrum of the backward SBL signal. (b) The RF beat note signal generated by mixing the pump light and the SBL. (c) Power of backward SBL as a function of the on-chip pump power.

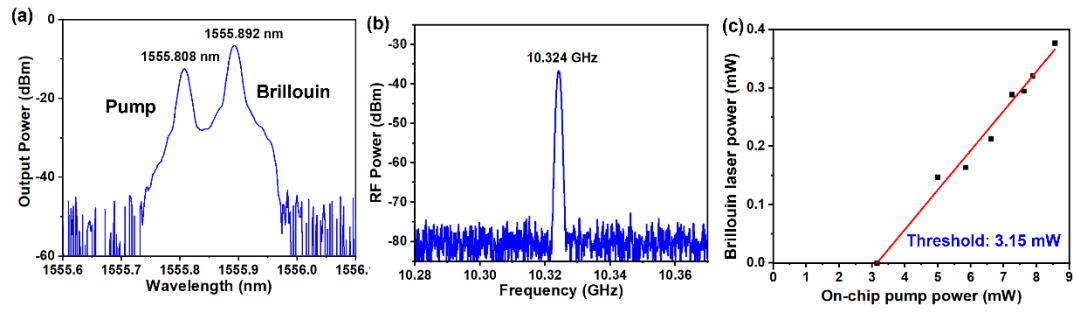
Fig. 3 (Color online) (a) Schematic diagram of backward SBL in resonator. The sign of azimuthal number means pump light and Stokes light propagate in opposite directions for backward scattering. (b) Modal dispersion of optical modes in LNOI microresonator. (c) Determined optical modes and acoustic mode with largest optomechanical coupling rates after considering phase matching condition and energy conservation.

Fig. 4 (Color online) (a) The frequency noise spectra of the pump light and the backward SBL. (b) Intrinsic linewidth of the backward SBL as a function of the SBL power.

Fig. 1



**Fig. 2**



**Fig. 3**

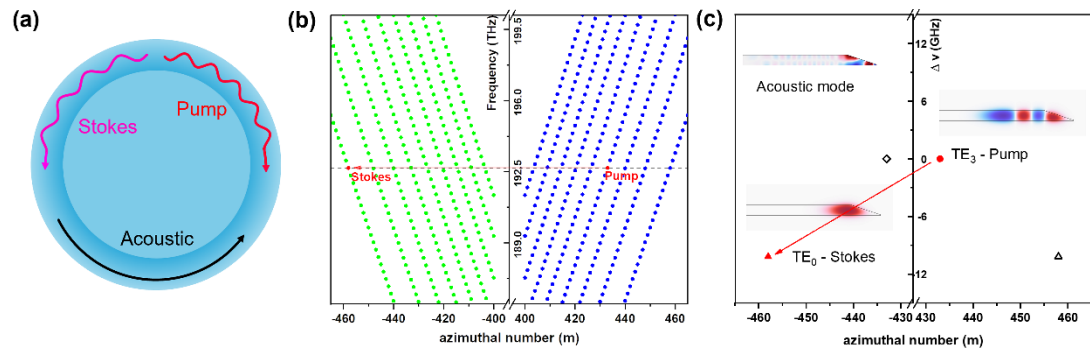




**Fig. 4**

